FISEVIER

Contents lists available at ScienceDirect

Progress in Organic Coatings

journal homepage: www.elsevier.com/locate/porgcoat





Sebaceous gland-inspired self-lubricated de-icing coating by continuously secreting lubricants

Yubo Liu^{a,d}, Weiming Sun^e, Kai Feng^c, Yang Wu^{b,c,d,*}, Bo Yu^b, Shujuan Liu^{a,**}, Feng Zhou^b

- a State Key Laboratory of Solidification Processing, Centre of Advanced Lubrication and Seal Materials, Northwest Polytechnical University, Xi'an, Shaanxi 710072, PR
- b State Key Laboratory of Solid Lubrication, Lanzhou Institute of Chemical Physics, Chinese Academy of Science, Lanzhou, Gansu 730000, PR China
- ^c Yantai Zhongke Research Institute of Advanced Materials and Green Chemical Engineering, Shandong Laboratory of Advanced Materials and Green Manufacturing, Yantai 264006. PR China
- ^d Qingdao Centre of Resource Chemistry and New Materials, Qingdao, Shandong 266100, PR China
- e Fujian Key Laboratory of Drug Target Discovery and Structural and Functional Research, School of Pharmacy, Fujian Medical University, Fuzhou, Fujian 350004, PR China

ARTICLE INFO

Keywords: Sebaceous gland Bioinspired Self-lubrication Continuous secretion De-icing

China

ABSTRACT

In recent years, oil-contained deicing materials have aroused peoples' concern due to their weak ice adhesion feature. Yet the loss of lubricant on oil-contained surface caused by contact or volatilization should be considered. Oily sebum secreted by sebaceous glands lubricates and moisturizes our skin, and can be reproduced continuously even after daily cleaning. In this work, inspired by sebaceous glands, a self-lubricant (SL) coating with ultra-low ice adhesion and excellent deicing durability was designed via continuously secreting lubricants. To determine the suitable simulant of oily sebum, the tribological tests and theoretical simulation analysis of lubricant on ice were conducted, confirming the effect of polydimethylsiloxane (PDMS) lubricants. By well mixing lubricant and resin, and sebaceous glands-like structures formed in coating matrix after curing, which endowed coating with lubricant storage feature and sebum-like secretion structure. The affinity of PDMS molecules to ice and the regeneration of lubricant film ensured the deicing durability of coating. Ice adhesion strength can be kept below 100 kPa even after 100 icing-deicing cycles, and can recover low ice adhesion strength (~50 kPa) via lubricant secreting. This work highlights the importance of lubricant selection and gives a new vision to designing durable icephobic materials.

1. Introduction

The freezing phenomena and accumulation of ice brings safety hazards in many fields such as winter transportation [1], wind turbines [2], aircraft [3], offshore platforms [4], high-speed railway and power transmission [5,6]. In order to prevent ice formation and avoid the losses caused by unexpected icing, anti-icing and deicing materials have been developed in recent years to reduce the hazards of ice accumulation [7–10]. Natural surfaces with special wettability have attracted great attention of researchers, and masses of bionic interface anti-icing and deicing materials were developed. Inspired by lotus leaves, superhydrophobic surfaces (SHSs) were built and applied on anti-icing [11–13]. On SHSs, water drops bounced and slid away off quickly due

to the air shield trapped on the surface, which avoided ice accumulation [14–16]. However, freezing phenomena was inevitable on SHSs in cold humid ambience and led to high ice adhesion strength due to the interlock effect between ice and SHSs [9]. Surface morphology of SHSs can be destroyed via mechanical deicing, which irreversibly decrease superhydrophobicity and anti-icing performances. To overcome the drawback of SHSs, external energy, such as, solar light [17–20] and electricity [17,21] were introduced to melt ice on SHSs to ensure non-destructive deicing. Bioinspired by *Nepenthes* pitcher plants, researchers developed various slippery liquid-infused porous surfaces (SLIPS) [22], and reported excellent anti-icing performance [23–26]. Lubricant impregnated in functional porous solid has not only created isotropic smooth surface to delay icing but also isolated the direct

E-mail addresses: yangwu@licp.cas.cn (Y. Wu), liusj@nwpu.edu.cn (S. Liu).

^{*} Correspondence to: Y. Wu, State Key Laboratory of Solid Lubrication, Lanzhou Institute of Chemical Physics, Chinese Academy of Science, Lanzhou, Gansu 730000, PR China.

^{**} Corresponding author.

contact of ice block and solid surface to reduce ice adhesion strength. Yet, lubricants on SLIPS drained inevitably by contact repeatedly or volatilization, which led to the loss of anti-icing performance [27-30]. Thus, series of durable anti-icing SLIPSs were developed by enhancing porous surface strength [31,32], or the interaction between lubrication molecules and surface [33-36], etc. Penguins lived in the Antarctica, but no ice was found on its skin. Researchers have found that the excellent anti-icing feature of penguin credit to the structure of feather and oily secretion [37,38]. Inspired by the chemical composition and structure of penguin's feathers, Wang et al. fabricated polyimide fiber membrane with water repellence characteristics. By choosing an effective distance between nanofiber, coalescence of microdroplets was prevented and anti-icing performance was achieved [37]. Besides, some insects and fishes can survive in subzero condition, which was contributed to themselves antifreeze protein that depress the freezing temperature by preventing heterogeneous ice nucleation [39,40]. Inspired by the ice nucleation suppression mechanism, AFPs mimics including polyampholytes, graphene oxide and polypeptides were developed for preventing ice formation [41,42].

Sebaceous glands are microscopic organs on human skin, they secrete sebum compound continuously to protect our skin by reducing moisture loss, inhibiting bacterial growth and lubricating skin to prevent skin scratch, etc. [43]. In this work, inspired by skin sebum secretion, a sebaceous glands-like self-lubricated (SL) icephobic coating that can secrete lubricants continuously to form lubrication layer was developed. Though lubricants were widely used to prepare the SLIPS materials, an important issue that how to select a suitable lubricant, was rarely considered. Experimental and theoretical analysis of two kinds of lubricants including poly-α-olefins (PAOs) and polydimethylsiloxane (PDMS) were considered, and found that PDMS was easier to form a stable oil film on ice surface, which shows a better lubricating performance than PAO lubricant. Thus, the PDMS lubricant acted as sebum simulant was used to prepare self-lubrication (SL) coating. In the coating matrix, numerous sebaceous gland-like porous structure that can regenerate lubricant layer from bulk to surface by the connected holes achieved long-term anti-icing. The PDMS lubricant film on SL coating surface can prevent the direct interaction between ice and surface, which can greatly reduce the ice adhesion strength. Both the lubricant with sustained secretion in sebaceous gland-like structure and the affinity of lubricant endowed coating with durable deicing property. The coating retained icephobic feature even after 100 icing-deicing cycles, and even if the surface lubricant was washed off with detergent, the coating can restore an ultra-low ice adhesion state by slowly releasing the lubricant at room temperature. The demonstrative experiments also confirmed the availability of SL coating in diverse application surroundings. This work provides a new perspective for designing durable icephobic coating.

2. Experimental section

2.1. Materials

Polydimethylsiloxane, hydroxypropyl silicone oil ($M_W \sim 2200$) were purchased from Shangdong Dayi Chemical CO., LTD. 2-Hydroxyethyl methacrylate (HEMA) and butyl acrylate were purchased from Shanghai Aladdin Bio-Chem Technology Co., LTD. Toluene diisocyanate (TDI) was purchased from TCI (Shanghai) Development Co., Ltd. Poly α olefins (PAOs) were purchased from Shanghai Dowpol Chemical International Co., Ltd. Xylene was purchased from Macklin, and azodiisobutyronitrile (AIBN) was purchased from J&K Scientific. Dibutyltin dilaurate (DBTDL) was purchased from Damao Chemical Reagent Factory. 2-Acetoxy-1-methoxypropane (PMA) was purchased from Aladdin and dewatered by magnesium sulfate before used.

2.2. Characterization

Viscosities of lubricants in low temperature were measured by a rheometer (HAKKE, RS6000) at −20 °C. Contact angles on ice of various lubricants were conducted on DECCA-100 optical contact-angle meter (DECCA precision instrument Co., LTD Shenzhen) and Laplace-Young algorithm was used to fitting CA values automatically, the test temperature was -20 °C. Scanning electron microscope (SEM) images were observed on a field emission scanning electron microscope (FESEM, JEOL JSM-6701F) at 5–10 kV. MFT-R4000 reciprocating friction and wear tester (Lanzhou Huahui) was used to measure the coefficient of friction (COF) on ice at various friction conditions as shown in Figs. 1a and S1. Ice with a smooth surface was prepared by cooler in advance. The mixture of acrylate prepolymer and silicone modified crosslinker was dropped on poly tetra fluoroethylene (PTFE) column with diameter at 6.4 mm and cured for 3 h at 50 °C, the cured silicone modified polyurethane (SPU) coating was used for tribological measurements. By varying the load and temperature, COFs of SPU on ice surface was measured to find a high COF friction condition for further lubricant selection as shown in Fig. S2, it was found that SPU slid on ice under 4 N and - 20 °C condition showed the highest COF as we measured. Lubrication performances of oils were measured by tribological tests with infinitesimal lubricants acted as medium to lubricate ice (4 N, −20 °C).

2.3. Synthesis of acrylate prepolymer

Monomer solution consisting of 6 g HEMA, 11 g butyl acrylate, 30 g xylene and 0.2 g AIBN was slowly added to solution of 4 g butyl acrylate and 10 g xylene under stirring at 80 $^{\circ}\text{C}$ for 2 h as shown in Fig. S3. The acrylate prepolymer with viscous state was obtained by reacting at 80 $^{\circ}\text{C}$ for another 4 h. The prepolymer solution was used to preparation SPU and self-lubricated (SL) coating without any treatment.

2.4. Synthesis of silicone modified crosslink agent

22 g hydroxypropyl silicone oil was slowly added to solution consisting of 3.4832 g TDI and anhydrous PMA with the existence of two drop dibutyltin dilaurate (DBTDL) under stirring tenderly at room temperature as shown in Fig. S4a. After 6 h, crosslink agent for silicone modified polyurethane was obtained. IR spectrum of silicone modified crosslink agent was shown in Fig. S4b.

2.5. Preparation of SPU and self-lubricated (SL) coating

SPU was obtained by mixing a certain quantity of acrylate prepolymer and silicone modified crosslinker, and the mixed solution was sprayed on steel test sheet to obtain a flat coating at 50 $^{\circ}$ C for 3 h. A certain quantity of SPU prepolymer was mixed with various contents of PDMS by ultrasonic dispersion for 0.5 h. After adding crosslinker, the mixture was sprayed on steel substrate and heating at 50 $^{\circ}$ C for 3 h, the self-lubricated (SL) coatings with 0 wt%, 13.74 wt%, 24.15 wt%, 32.33 wt%, 38.91 wt% and 44.32 wt% lubricant contents were prepared.

2.6. Ice adhesion strength test

A laboratory-made ice adhesion tester was used to measure ice adhesion strength. As shown in Fig. 3a, the tester meanly consists of three parts, including motion control system, cooler and force sensor. Cryogenic circulator was used to obtain testing temperature of $-20\,^{\circ}\text{C}.$ Coating was precooled on cooler and 2 mL deionized water was froze in a 2 cm * 2 cm square mold for 1 h before tests. Mechanical force paralleled to coating was conducted on mold to peel off ice cube with velocity of 0.001 m/s. The force (Fice) needed for removing ice cube was measured by a force sensor. Ice adhesion strength (τ_{ice}) is calculated according to formula as follows:

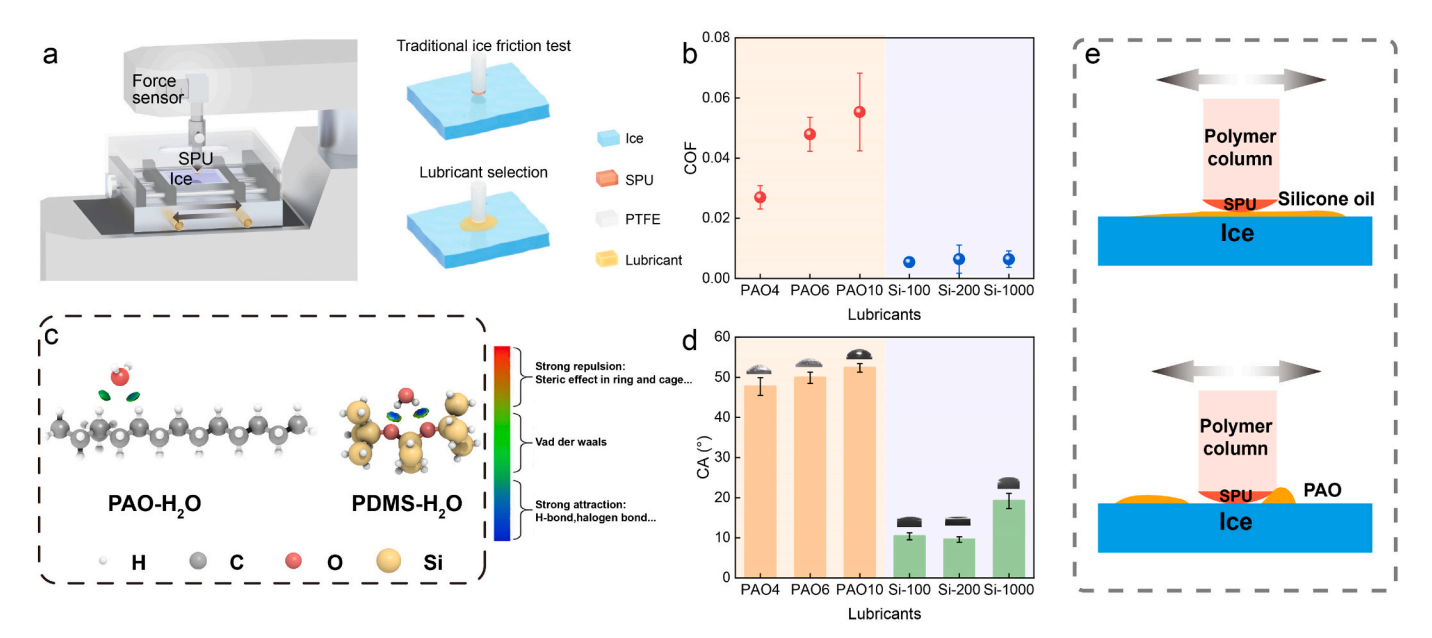


Fig. 1. (a) Schematic of ice friction tester. (b) The COFs on ice surface with different lubricants (load 4 N, frequency 1 Hz). (c) The IGMH figures of the most stable PAO-H₂O and Si-H₂O complexes. (d) The CAs of lubricants on ice. (e) Schematic of the lubricating film on ice for two lubricants.

$$\tau_{ice} = \frac{F}{S} \tag{1}$$

Among them, τ_{ice} is ice adhesion strength, F is the shear force needed to remove ice and S is the contact area between ice and sample surface.

2.7. Deicing durability test

Deicing durability test was conducted at the same condition as shown in ice adhesion strength test. Water freezing in ice and the measurement of ice adhesion strength was taken as an icing-deicing cycle. The durability of SL coating was taken by repeatedly carry out the icing-deicing cycles.

2.8. Theoretical stimulation of the interaction between water and lubricant molecules

Firstly, Minnesoda functions (M06-2X) [44–46] and 6-311+G(d,p) basis set [44–46] were used to optimize the geometry structure of PAO-H₂O and PDMS-H₂O complexes. The vibration frequency analysis was conducted at the same level to make sure all the optimized structures were the smallest at the potential energy surfaces respectively. The combination of M06-2X functional and Pople basis set was widely used to study the weak interaction of non-covalent systems [47–50]. After that, we calculated the interaction of energy (E_{int}) at the same level for the lowest-energy PAO-H₂O and PDMS-H₂O complexes by using the formula,

$$E_{int} = E(X - H_2O) - E(X) - E(H_2O)$$
 (2)

where E (X-H₂O), E (X) and E (H₂O) are the electron energies of the most stable compound X-H₂O, X and H₂O, respectively. Herein, the basis-set superposition error (BSSE) correction has been considered by using the counterpoise method [51]. In order to deeply understand the nature of the bonds between PAO/PDMS and water, the independent gradient model based on Hirshfeld electron density distribution (IGMH) [52] figures of the obtained complexes were also analyzed. All the above calculations are performed using Gaussian 16 software [53]. The GaussView program [53] is used to obtain the geometric structures. The Multiwfn program is used to obtain IGMH isosurface maps [53].

3. Results and discussion

3.1. Tribological measurements for lubricant selection

Before the SL coating preparation, the suitable lubricant was considered at first. In this work, the friction behaviors of lubricants on ice were tested for oily lubricant selection. The schematic of friction process on ice was drawn in Fig. 1a. The SPU coating attached on PTFE pin was used as the upper friction pair, and infinitesimal PAO or PDMS was acted as the medium to lubricate ice surface. The friction coefficients (COFs) of poly α -olefins (PAOs) and polydimethylsiloxane (PDMS) were shown in Fig. 1b. Interestingly, the COFs of PAOs on ice surface risen from 0.027 \pm 0.004 to 0.055 \pm 0.013 with the increase of structural unit that affects the viscosity of PAO (Table S1). But for PDMS lubricant, an ultra-low one-tenth of COF was presented and remained nearly constant at \sim 0.005 \pm 0.003, which was free from the influence of viscosity of PDMS.

To explore the reason for the difference in the lubrication performance of these two types of lubricants, the interaction between lubricant molecule and water molecule was studied by density functional theory (DFT) calculations. The most stable structures of X-H₂O (X = PAO/PDMS) are obtained and shown in Fig. S5. In the PAO-H₂O complex, H₂O molecule combined with two hydrogens on the alkane through its oxygen atom to form O...H bonds with bond lengths of 2.146 and 2.004 Å, respectively. The interaction energy (E_{int}) between H₂O and PAO was 2.31 kcal/mol that indicates heat absorption and unstable interaction. On the contrary, the E_{int} between H₂O and PDMS was -5.74kcal/mol, indicating that the binding process was exothermic and stable interaction. Moreover, the two H···O intermolecular bonds formed between H₂O and PDMS were as short as 1.755 and 1.740 Å. The shorter bonds and negative interaction energy indicated that H₂O molecule was more inclined to combine with PDMS. To intuitively visualize the weak interaction, the independent gradient model based on Hirshfeld electron density distribution (IGMH) figures were also obtained and plotted in Fig. 1c, where the isosurface color of the hydrogen bond formation region in PDMS-H₂O was obviously blue, indicating the strong electrostatic attraction between them. But for PAO-H2O, the dominant green zones demonstrated the wear Van der Waals interaction between PAO and H₂O molecules. Thus, as compared to PAO lubricant, PDMS was easier to combine with H2O through hydrogen bonds to form stable PDMS- $\rm H_2O$ complexes. In other words, PDMS can form more stable lubricant layers on ice than PAOs, thus a lower COF on ice surface was presented.

The static contact angle of lubricants on ice surface also confirmed their affinity. As shown in Fig. 1d, the contact angle of PAO droplet was about $47.7\pm2.2^{\circ}$, which showed the lowest CA among the tested PAOs. But the contact angles of PDMS droplets were $<\!20^{\circ}$. The CA value means PDMS lubricant wetted ice surface to form a stable oily lubricating film easily. Therefore, we deduced that it was hard to form a complete and stable lubricating film on ice surface when lubricated by PAOs. The PAO adhered on the friction pin and wetted ice surface mildly due to its weak interaction between lubricant and water molecules. And the PAO with high viscosity was more easily to hinder the movement of friction pin, which led to a high friction coefficient. But for PDMS, the lubricant

wetted the ice surface quickly, and stable and homogeneous lubricating film formed at the friction interface. Hardly any PDMS lubricant adhered on the friction pin, thus the COF of PDMS on ice was independent on its viscosity (Fig. 1e). From the above analysis, the conclusion can be concluded that PDMS lubricant can form a complete and stable lubricant film on ice surface, and effectively avoid direct interaction between ice and substrate to reduce the ice adhesion strength.

3.2. Preparation of SL coating

Thus, inspired by sebaceous gland on our skin, the self-lubrication (SL) coating with self-secretion lubricant was proposed, which PDMS was acted as sebum simulant. Fig. 2a shows the preparation process of SL coating. Acrylic resin, silicone polyisocyanate curing agent and PDMS

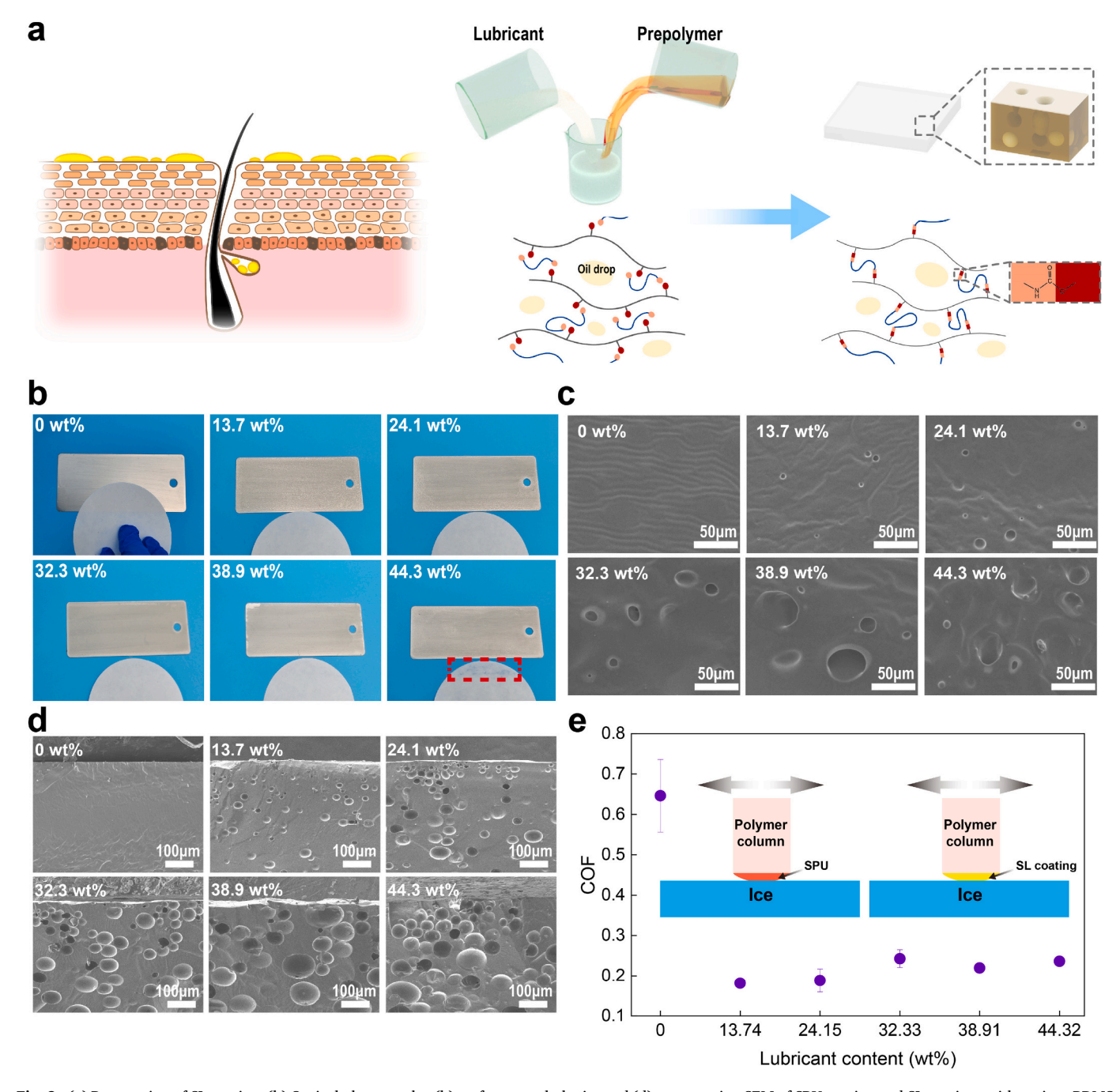


Fig. 2. (a) Preparation of SL coating. (b) Optical photographs, (b) surface morphologies and (d) cross section SEM of SPU coating and SL coatings with various PDMS contents. (e) The friction coefficient of SPU coating and SL coatings on ice surface (-20 °C, 4 N, 2 Hz).

lubricant were dissolved and mixed violently in the right amount of solvent. The mixture was sprayed on substrate surface and cured at 50 $^{\circ}\text{C}$ for 3 h to obtain SL coating. The sebaceous-gland-like porous structure in SL coating formed by phase separation and solvent evaporation in curing process. Fig. 2b shows the optical photograph of SL coating with different PDMS contents. The filter paper touched to the SL coating surfaces to judge the lubricant secretion, and only obvious oil mark was observed on the SL coating contained with 44.3 wt% PDMS content. Surface and cross-sectional morphologies of SL coatings were also detected by scanning electron microscope (Fig. 2c and d). As shown in Fig. 2c, the SL coating without PDMS lubricant exhibits smooth surface without holes, while holes with tiny holes ranging from 10 to 40 μm appears when PDMS lubricant content increase above 13.7 wt%. With the lubricant content increase in SL coating, the size and number of holes were also increased. Fig. 2d demonstrates the cross-sectional SEM images of SL coating clearly. With the increase of lubricant content, the size and number of interpenetrated vesicles became larger, which indicated plentiful of impregnated PDMS lubricant secretion and resulted in the macroscopical oil mark on SL coating (Fig. 2b). To confirm the lubrication of SL coatings, their friction performances on ice surface were conducted under -20 °C. The SL coating attached to the upper friction pin, and slid on ice surface under 4 N load. The friction coefficient was summarized in Fig. 2e, and found that SL coating surface has a lower friction coefficient (\sim 0.20) than that of SPU coating surface (\sim 0.65). The significant difference of friction coefficient can be attributed to the rapid formation of PDMS lubricant film on the friction zone with reciprocating friction of SL coating surface.

3.3. Durability of de-icing

Ice adhesion strength was widely used to evaluate the deicing performance. Here, a laboratory-made device was used to measure the peak force of ice shedding to calculate ice adhesion strength (Fig. 3a), and the ice adhesion strength of SL coatings with various PDMS lubricant contents were summarized in Fig. 3b. Ice adhesion strength on the SPU coating was 347.9 \pm 32.8 kPa, and the adhesion strengths gradually decreased with the increase of lubricant. The lowest ice adhesion strength was found on SL coating with 44.32 wt% lubricant content that

was as low as 5.2 \pm 1.8 kPa. With the increase of lubricant, more free lubricant was found on coating surface, greatly decreased the contact area between ice and substrate which endowed easily deicing feature. The durability of deicing performance was conducted on the SL coating with 44.32 wt% lubricant content. After 100 icing-deicing cycles, the ice adhesion strengths gradually increased to about 90 kPa (Fig. 3c), which indicates the destruction of lubricating film between ice and coating surface after repeatedly contact-detach cycles. In consideration of the actual application scenario, the coating surface would be contaminated by dust or washed by detergent. So, for above conditions, the ice adhesion strength on dust covered SL coating surface and washed SL coating surface were tested. The results were summarized in Fig. 3d and the low ice adhesion strengths, 51.6 \pm 25.9 kPa for detergent washed surface and 24.5 \pm 2.1 kPa for dust covered surface, were showed, respectively. The resistance to water flow washing of SL coating was also measured. The SL coating surface was fixed on a mechanical agitator and rotated with 200 r/min in water, and ice adhesion strengths were tested after washing with a period of time to evaluate the anti-water flow ability. As shown in Fig. 3e, ice adhesion strength rose slowly with the increase of water washing time, and after 34 h water flushing the ice adhesion strength increased to 99.1 \pm 27.9 kPa. In addition, the recovery of icephobicity is the most important features for SL coating. The PDMS lubricant secreted from SL coating matrix to guarantee low ice adhesion strength even the surface lubricant was rinsed cleanly by ethanol. As shown in Fig. 3f, the ice adhesion of SL coating raised to 175 kPa rapidly after washing by ethanol, while reduced to 80 kPa after left at room temperature for one day. With the increase of days, the ice adhesion also reduced slowly. Lubricant stored in vesicles might gradually spread and secrete to coating surface, like sebaceous glands secreted sebum as shown in Fig. 3g. The surface lubricant was gradually regenerated and ice adhesion strength was as low as 29.8 \pm 3.0 kPa after placing coating at room temperature for 30 days. As shown in Fig. 3h, the initial ice adhesion strength of SL coating was pretty low ($\tau_{ice} < 10$ kPa) and we have measured the most durable deicing tests cycles compared with other oily lubricant anti-icing surfaces [54–59]. With the existence and regeneration of surface lubricant layer, SL coating showed excellent deicing performance and durability.

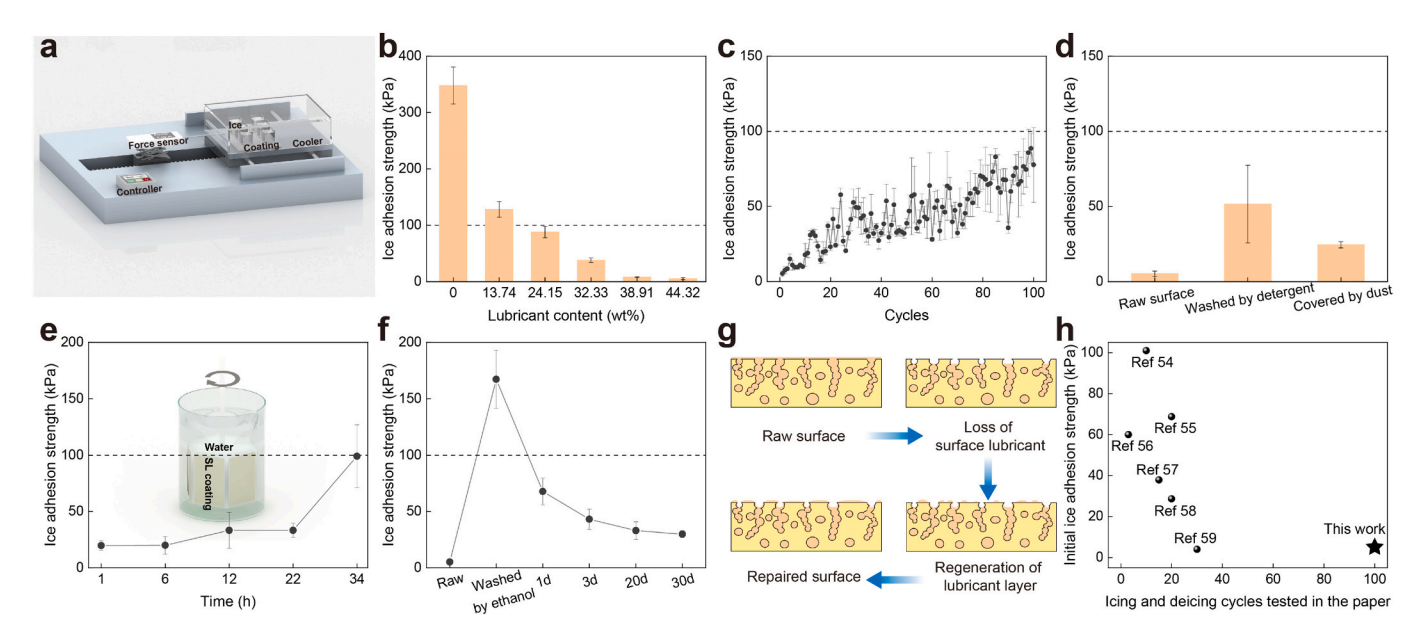


Fig. 3. (a) Scheme of lab-made ice adhesion strength measurement device. (b) Ice adhesion strength on coating with various PDMS contents. (c) Deicing durability test of SL coating. (d) Ice adhesion strengths of raw SL coating surface, detergent washed SL coating surface and dust covered SL coating surface. (e) Ice adhesion strengths of SL coating after water flow washing at different times. (f) Icephobicity recovery of SL coating after ethanol washing at room temperature. (g) Illustration of icephobic recovery of SL coating. (h) Comparison of the initial ice adhesion strength and icing/deicing cycles tested between SL coating and typical oily lubricant impregnated anti-icing materials [54–59].

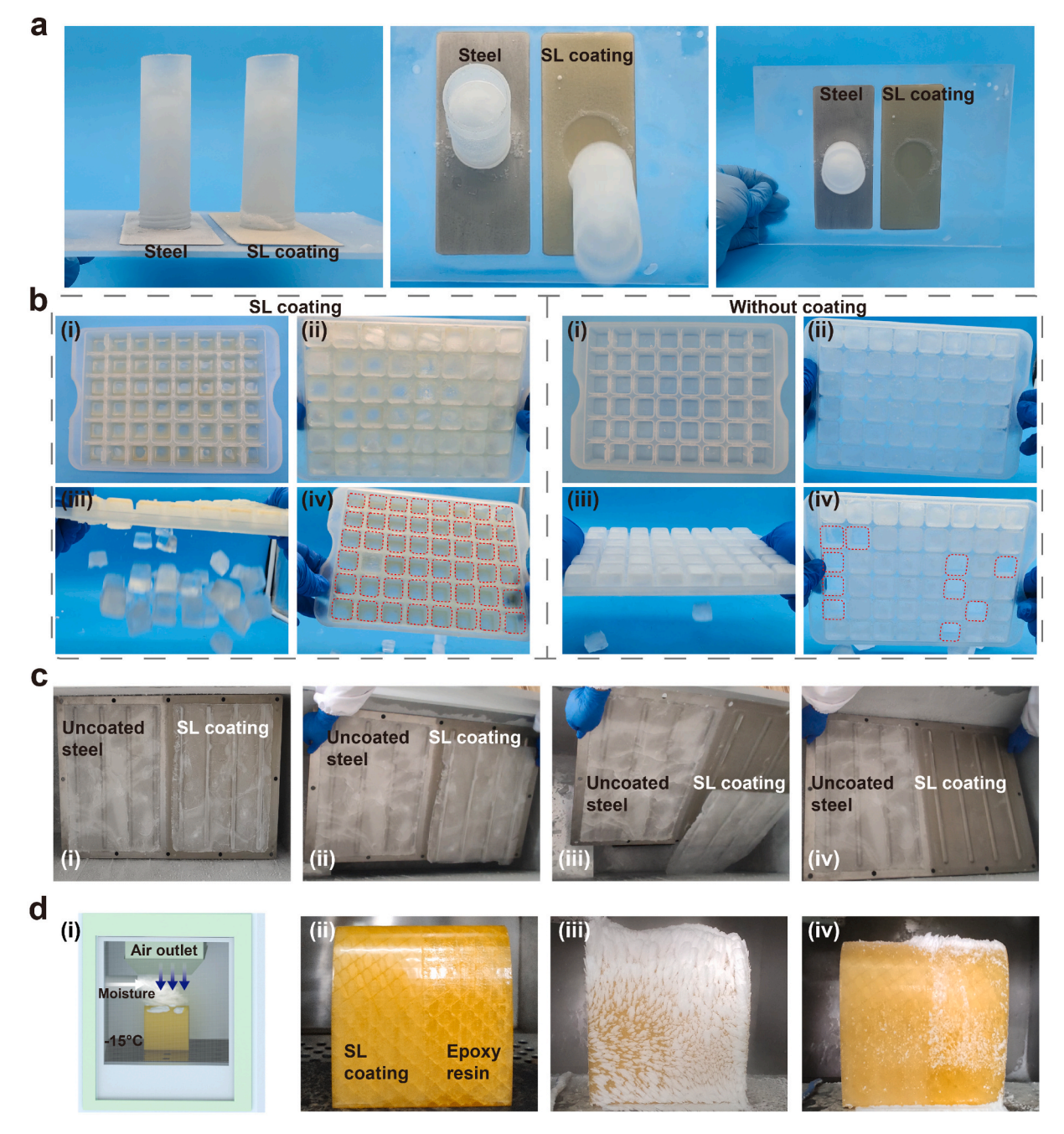


Fig. 4. (a) Ice shedding by gravity on steel and SL coating surfaces. (b) Ice cubes falling process on SL coating treated tray and uncoated tray. (c) Large-scale deicing on steel and SL coating. (d) Scheme and photographs of defrosting in cold windy environment.

3.4. Deicing performance

To confirm the usability of SL coating, some application proof tests were conducted. As shown in Fig. 4a and Movie S1, ice pillar frozen on SL coating surface can fall off by its own gravity when put the surface vertically, yet it cannot fall off on steel surface due to the strong adhesion between ice and steel surface. The cube tray was coated with SL coating, and the ice cubes frozen in refrigerator ($-30\,^{\circ}\text{C}$) for one night. Almost all ice cubes fall off from the cube tray coated with SL coating when overturned, while it was hard to fall off from the bare cube tray and stay tightly on it even twisted many times (Fig. 4b and Movies S2, S3). Large-scale deicing performance of SL coating was also presented. A half of steel plate with 60 * 90 cm was painted with the SL coating, and as a contrast, the other half of steel plate was naked. Amount of water poured on the steel plate surface and frozen in $-30\,^{\circ}\text{C}$ for 24 h, as shown

in Fig. 4c and Movie S4, the ice layer fell off entirely from SL coating surface when we took the steel plate from refrigerator, but the ice layer attached on the steel surface tightly. The defrosting ability in cold windy environment at the temperature of $-15\,^{\circ}\mathrm{C}$ was further tested to simulate the working environment of airplane. As shown in Fig. 4d, the half area of airplane wing model was covered by SL coating and the other half place was covered by epoxy resin. Wing model was placed in a cold humid environment for 30 min, and the surface was covered with frost, as shown in Fig. 4d. After frosting, wind with velocity of $\sim\!28\,\text{m/s}$ blown on the wing model for 10 min. Frost on SL coating was approximately removed by wind, yet residual frost was found on epoxy covered surface, which was owing to the low ice adhesion strength on SL coating surface.

4. Conclusion

In this work, bioinspired from sebaceous gland, a self-lubricated (SL) coating with ultra-low ice adhesion strength and excellent durability was fabricated. To find the optimal sebum simulant, the lubrication performances and mechanism of two series oils, including PAO and PDMS, on ice were considered firstly. Experimental and theoretical simulation results confirmed the differences of lubrication performances and figured out that PDMS had better affinity to ice surface than PAO, which guaranteed the formation of PDMS lubricative film on ice surface to reduce COF. Thus, the PDMS lubricant was selected as sebum simulant to prepare sebaceous gland-like SL coating. The PDMS in SL coating can also form a complete oil film to reduce the direct contact between ice and another surface owing to the good ice affinity, therefore, greatly decreased the ice adhesion strength(<100 kPa). With the existence of sebaceous gland-like structure, SL coating possessed self-recover performance. And the SL coating with low ice adhesion strength and long service life showed broad application prospect in de-icing area. The oil selection and SL coating designation may provide universal ideas for icephobic materials.

Supplementary data to this article can be found online at https://doi.org/10.1016/j.porgcoat.2022.107311.

CRediT authorship contribution statement

YANG WU proposed the idea and supervised the research. YUBO LIU, KAI FENG, YANG WU, BO YU, SHUJUAN LIU, and FENG ZHOU designed the experiment. WEIMING SUN performed the theoretical calculation. YUBO LIU and FENG KAI performed the experiments, collected the data, and prepared the figures. YUBO LIU, FENG KAI, YANG WU and SHUJUAN LIU wrote the manuscript. All the authors discussed the manuscript.

Declaration of competing interest

The authors declared that they have no conflicts of interest to this work

Data availability

Data will be made available on request.

Acknowledgment

The authors gratefully acknowledge the support by the NSAF (Grant No. U2030201), the National Key Research and Development Program of China (2020YFF0304600), the LICP Cooperation Foundation for Young Scholars (HZJJ22-07), Young Talents Support Plan of Gansu Association for Science and Technology (GXH2020626-14).

References

- [1] A. Jean, M. Brian, JV, Institute for Catastrophic Loss Reduction, 2001.
- [2] O. Parent, A. Ilinca, Cold Reg. Sci. Technol. 65 (2011) 88-96.
- [3] S. Thomas, R. Cassoni, C.Mac Arthur, 34th Aerospace Sciences Meeting and Exhibit, 1996.
- [4] C.C. Ryerson, Cold Reg. Sci. Technol. 65 (2011) 97–110.
- [5] M. Farzaneh, C. Volat, A. Leblond, Anti-icing and de-icing techniques for overhead lines, in: M. Farzaneh (Ed.), Atmospheric Icing of Power Networks, Springer, Dordrecht, 2008, pp. 229–268.
- [6] T. Li, J. Li, CIRED 20 th International Conference on Electricity Distribution, 2009.
- [7] Y. Liu, Y. Wu, S. Liu, F. Zhou, ACS Mater. Lett. 4 (2022) 246-262.
- [8] Y. Zhuo, S. Xiao, A. Amirfazli, J. He, Z. Zhang, Chem. Eng. J. 405 (2021), 127088.
- [9] J. Lv, Y. Song, L. Jiang, J. Wang, ACS Nano 8 (2014) 3152–3169.
- [10] A. Dhyani, J. Wang, A.K. Halvey, B. Macdonald, G. Mehta, A. Tuteja, Science 373 (2021), eaba5010.

- [11] L. Mishchenko, B. Hatton, V. Bahadur, J.A. Taylor, J. Aizenberg, ACS Nano 4 (2010) 7699–7707.
- [12] J.C. Bird, R. Dhiman, H.M. Kwon, K.K. Varanasi, Nature 503 (2013) 385-388.
- [13] Y. Liu, L. Moevius, X. Xu, T. Qian, J.M. Yeomans, Z. Wang, Nat. Phys. 10 (2014) 515–519.
- [14] D. Vollmer, H.-J. Butt, Nat. Phys. 10 (2014) 475-476.
- [15] D. Richard, C. Clanet, D. Quéré, Nature 417 (2002) 811-812.
- [16] X. Wang, H. Hu, Q. Ye, T. Gao, F. Zhou, Q. Xue, J. Mater. Chem. 22 (2012) 9624–9631.
- [17] T. Hao, Z. Zhu, H. Yang, Z. He, J. Wang, ACS Appl. Mater. Interfaces 13 (2021) 44948–44955.
- [18] B. Yu, Z. Sun, Y. Liu, Z. Zhang, Y. Wu, F. Zhou, ACS Appl. Mater. Interfaces 13 (2021) 37609–37616.
- [19] M.I. Jamil, X. Zhan, F. Chen, D. Cheng, Q. Zhang, ACS Appl. Mater. Interfaces 11 (2019) 31532–31542.
- [20] Y. Liu, Y. Wu, Y. Liu, R. Xu, S. Liu, F. Zhou, ACS Appl. Mater. Interfaces 12 (2020) 46981–46990.
- [21] Y. Liu, R. Xu, N. Luo, Y. Liu, Y. Wu, B. Yu, S. Liu, F. Zhou, Adv. Mater. Technol. 6 (2021) 2100371.
- [22] T.S. Wong, S.H. Kang, S.K. Tang, E.J. Smythe, B.D. Hatton, A. Grinthal, J. Aizenberg, Nature 477 (2011) 443–447.
- [23] P. Kim, T.-S. Wong, J. Alvarenga, M.J. Kreder, W.E. Adorno-Martinez, J. Aizenberg, ACS Nano 6 (2012) 6569–6577.
- [24] F. Wang, Y. Zhuo, Z. He, S. Xiao, J. He, Z. Zhang, Adv. Sci. (Weinh.) 8 (2021), e2101163.
- [25] Y. Ru, R. Fang, Z. Gu, L. Jiang, M. Liu, Angew. Chem. Int. Ed. 59 (2020) 11876–11880.
- [26] X. Yin, Y. Zhang, D. Wang, Z. Liu, Y. Liu, X. Pei, B. Yu, F. Zhou, Adv. Funct. Mater. 25 (2015) 4237–4245.
- [27] S. Peppou-Chapman, J.K. Hong, A. Waterhouse, C. Neto, Chem. Soc. Rev. 49 (2020) 3688–3715.
- [28] S. Peppou-Chapman, C. Neto, Langmuir 37 (2021) 3025-3037.
- [29] S.B. Subramanyam, K. Rykaczewski, K.K. Varanasi, Langmuir 29 (2013) 13414–13418.
- [30] L.B. Boinovich, E.V. Chulkova, K.A. Emelyanenko, A.G. Domantovsky, A. M. Emelyanenko, J. Colloid Interface Sci. 609 (2022) 260–268.
- [31] C. Liu, Y. Li, C. Lu, Y. Liu, S. Feng, Y. Liu, ACS Appl. Mater. Interfaces 12 (2020) 25471–25477.
- [32] J. Zhang, C. Gu, J. Tu, ACS Appl. Mater. Interfaces 9 (2017) 11247-11257.
- [33] M. Tenjimbayashi, R. Togasawa, K. Manabe, T. Matsubayashi, T. Moriya, M. Komine, S. Shiratori, Adv. Funct. Mater. 26 (2016) 6693–6702.
- [34] R. Togasawa, M. Tenjimbayashi, T. Matsubayashi, T. Moriya, K. Manabe, S. Shiratori, ACS Appl. Mater. Interfaces 10 (2018) 4198–4205.
- [35] G.H. Zhu, S.H. Cho, H. Zhang, M. Zhao, N.S. Zacharia, Langmuir 34 (2018) 4722–4731.
- [36] Y. Tsuge, T. Moriya, Y. Moriyama, Y. Tokura, S. Shiratori, ACS Appl. Mater. Interfaces 9 (2017) 15122–15129.
- [37] S. Wang, Z. Yang, G. Gong, J. Wang, J. Wu, S. Yang, L. Jiang, J. Phys. Chem. C 120 (2016) 15923–15929.
- [38] E. Alizadeh-Birjandi, F. Tavakoli-Dastjerdi, J.S. Leger, K.F. Faull, S.H. Davis, J. P. Rothstein, H. Pirouz Kavehpour, Eur. Phys. J. Spec. Top. 229 (2020) 1881–1896.
- [39] T. Sun, F.H. Lin, R.L. Campbell, J.S. Allingham, P.L. Davies, Science 343 (2014) 795–798.
- [40] S.P. Graether, M.J. Kuiper, S.M. GagneÂ, V.K. Walker, Z. Jia, B.D. Sykes, P. L. Davies, Nature 406 (2000) 325–328.
- [41] G. Bai, D. Gao, Z. Liu, X. Zhou, J. Wang, Nature 576 (2019) 437-441.
- [42] Y. Zhang, K. Liu, K. Li, V. Gutowski, Y. Yin, J. Wang, A.C.S. Appl, Mater. Interfaces 10 (2018) 1957–1962.
- [43] R. Reuter, Aust. Vet. J. 85 (2007) 310.
- [44] R. Ditchfield, W.J. Hehre, J.A. Pople, J. Chem. Phys. 54 (1971) 724–728.
- [45] Y. Zhao, D.G. Truhlar, Theor. Chem. Accounts 120 (2008) 215-241.
- [46] N. Mardirossian, M. Head-Gordon, J. Chem. Theory Comput. 12 (2016) 4303–4325.
- [47] T. Dudev, S. Ilieva, L. Doudeva, Phys. Chem. Chem. Phys. 20 (2018) 24633–24640.
- [48] M. Walker, A.J. Harvey, A. Sen, C.E. Dessent, J. Phys. Chem. A 117 (2013) 12590–12600.
- [49] T. Sadhukhan, D. Das, P. Kalekar, V. Avasare, S. Pal, J. Phys. Chem. A 121 (2017) 4569–4577.
- [50] V. Barone, M. Cossi, J. Phys. Chem. A 102 (1998) 1995–2001.
- [51] S.F. Boys, F. Bernardi, Mol. Phys. 19 (1970) 553-566.
- [52] C. Lefebvre, H. Khartabil, J.C. Boisson, J. Contreras-Garcia, J.P. Piquemal, E. Henon, ChemPhysChem 19 (2018) 724–735.
- [53] T. Lu, F. Chen, J. Comput. Chem. 33 (2012) 580–592.
- [54] Y. Zhuo, F. Wang, S. Xiao, J. He, Z. Zhang, ACS Omega 3 (2018) 10139-10144.
- [55] S. Zheng, D.A. Bellido-Aguilar, X. Wu, X. Zhan, Y. Huang, X. Zeng, Q. Zhang, Z. Chen, ACS Sustain. Chem. Eng. 7 (2018) 641–649.
- [56] Y. Wang, X. Yao, S. Wu, Q. Li, J. Lv, J. Wang, L. Jiang, Adv. Mater. 29 (2017) 1700865.
- [57] Q. Liu, Y. Yang, M. Huang, Y. Zhou, Y. Liu, X. Liang, Appl. Surf. Sci. 346 (2015) 68–76.
- [58] F. Wang, W. Ding, J. He, Z. Zhang, Chem. Eng. J. 360 (2019) 243-249.
- [59] T. Li, Y. Zhuo, V. Håkonsen, S. Rønneberg, J. He, Z. Zhang, Coatings 9 (2019) 602.